

## 3I/ATLAS: In Search of the Witnesses to Its Voyage

X. PÉREZ-COUTO ,<sup>1,2</sup> S. TORRES ,<sup>3</sup> E. VILLAVER ,<sup>4,5</sup> A. J. MUSTILL ,<sup>6</sup> AND M. MANTEIGA ,<sup>7,2</sup>

<sup>1</sup>Universidade da Coruña (UDC), Department of Computer Science and Information Technologies, Campus de Elviña s/n, 15071, A Coruña, Galiza, Spain

<sup>2</sup>CIGUS CITIC, Centre for Information and Communications Technologies Research, Universidade da Coruña, Campus de Elviña s/n, 15071 A Coruña, Galiza, Spain

<sup>3</sup>Institute of Science and Technology Austria (ISTA), Am Campus 1, A-3400 Klosterneuburg, Austria

<sup>4</sup>Instituto de Astrofísica de Canarias, 38200 La Laguna, Tenerife, Spain

<sup>5</sup>Universidad de La Laguna (ULL), Astrophysics Department, 38206 La Laguna, Tenerife, Spain

<sup>6</sup>Lund Observatory, Department of Astronomy and Theoretical Physics, Lund University, Box 43, 221 00, Lund, Sweden

<sup>7</sup>Universidade da Coruña (UDC), Department of Nautical Sciences and Marine Engineering, Paseo de Ronda 51, 15011, A Coruña, Galiza, Spain

### ABSTRACT

3I/ATLAS is the third interstellar object discovered to date, following 1I/‘Oumuamua and 2I/Borisov. Its unusually high excess velocity and active cometary nature make it a key probe of the Galactic population of icy planetesimals. Understanding its origin requires tracing its past trajectory through the Galaxy and assessing the possible role of stellar encounters, both as a potential origin and a perturber to its orbit. We integrated the orbit of 3I/ATLAS backward in time for 10 Myr, together with a sample of *Gaia* DR3 stars with high-quality astrometry and radial velocities, to identify close passages within 2 pc. We identify 93 nominal encounters, 62 of which are significant at the  $2\sigma$  level. However, none of these encounters produced any meaningful perturbation. The strongest perturber *Gaia* DR3 6863591389529611264 at 0.30 pc and with a relative velocity of  $35 \text{ km s}^{-1}$ , imparted only a velocity change of  $|\Delta v| \simeq 5 \times 10^{-4} \text{ km s}^{-1}$  to the orbit of 3I/ATLAS. Our results indicate that no stellar flybys within the past 10 Myr and 500 pc contained in *Gaia* DR3 can account for the present trajectory of 3I/ATLAS or be associated with its origin. We further show that 3I/ATLAS is kinematically consistent with a thin-disk population, despite its large peculiar velocity.

**Keywords:** Interstellar objects (52), *Gaia* (2360), Milky Way dynamics (1051), Astrometry (80), Close encounters (255)

### 1. INTRODUCTION

Kinematics is the key to identify interstellar objects (ISOs), since their trajectories provide the most direct evidence of an extrasolar origin. Unlike asteroids and comets formed within the Solar System, which remain confined to bound elliptical, or near-parabolic, orbits ( $e \lesssim 1$ ), ISOs arrive with velocities at infinity and thus follow hyperbolic trajectories ( $e > 1$ ), with velocities determined by the Sun’s motion through the Galaxy and the distribution of velocities of the ISO population. Such kinematic signatures provide a robust diagnostic, rendering ISOs clearly distinguishable from native Solar System populations.

Email: xabier.perez.couto@udc.gal, santiago.torres@ist.ac.at

The discovery of the  $\sim 100$  m-sized 1I/‘Oumuamua by the Pan-STARRS survey (K. J. Meech et al. 2017) was long anticipated, as planet formation models predict the ejection of large amounts of material from the outer regions of forming planetary systems into interstellar space (e.g. S. N. Raymond et al. 2018). The efficiency of planetesimal ejection is highly sensitive to planetary architecture and dynamical history, yet dynamical models indicate that clearing processes are common across a wide range of system architectures. As a result, interstellar space should be filled with planetesimals originating in protoplanetary disks, predominantly icy in composition given that the majority of ejected material is expected to form beyond the snow line of their parent systems.

The discovery of 1I/‘Oumuamua confirmed the existence of ISOs and highlighted their value as tracers of planet formation efficiency and the density of small bod-

ies in the interstellar medium. Since then, two additional ISOs have been identified: 2I/Borisov (J. de León et al. 2019) and, most recently, 3I/ATLAS (D. Z. Seligman et al. 2025). The latter exhibits an extremely hyperbolic heliocentric orbit with eccentricity  $\sim 6.1$  and an incoming velocity of  $\sim 58 \text{ km s}^{-1}$ , along with clear evidence of water-ice activity and CO<sub>2</sub> emission (Z. Xing et al. 2025; C. M. Lisse et al. 2025), strongly suggesting an origin in the outer icy reservoir of another planetary system.

Identifying the origin of ISOs is key to understanding planet formation efficiency, the distribution of volatiles and organics in the Galaxy, and the dynamical pathways by which planetary systems evolve. Proposed origins range from early ejection during planet formation (A. Do et al. 2018; S. Portegies Zwart et al. 2018), to scattering in intermediate-age systems (R. Brasser & A. Morbidelli 2013; S. N. Raymond et al. 2018; Torres, S. et al. 2023), to late-stage release by stellar perturbations or post-main-sequence mass loss (J. J. Jiménez-Torres et al. 2011; A. Higuchi & E. Kokubo 2015; Torres, S. et al. 2019; D. Veras et al. 2011; D. Veras & C. A. Tout 2012). More exotic models have also been suggested, including tidal fragmentation of comets (Y. Zhang & D. N. C. Lin 2020), formation in molecular cloud cores (W. G. Levine & G. P. Laughlin 2021), and tidal disruption of asteroids around white dwarfs (R. R. Rafikov 2018).

The unusually high excess velocity of 3I/ATLAS has already motivated attempts to constrain its origin using age–velocity relations and Galactic dynamics (M. J. Hopkins et al. 2025b; A. G. Taylor & D. Z. Seligman 2025; R. de la Fuente Marcos et al. 2025; S. Kakharov & A. Loeb 2025; Y. Guo et al. 2025). If the chemical abundances and Galactic dynamics of a sample of ISOs are both sufficiently constrained, it would allow tests of correlations between kinematics and compositions expected from Galactic chemodynamics models, and hence allow us to probe the compositions of planetary building blocks across space and time in the Galaxy (M. J. Hopkins et al. 2023, 2025a). In a very fortuitous case, a reconstruction of the ISO’s past Galactic orbit—coupled with those of nearby stars—could reveal the original parent star of the ISO<sup>8</sup>. Moreover, encounters with other stars can gravitationally perturb ISO trajectories (e.g., J. Heisler & S. Tremaine 1986; H. Rickman 2014; F. Feng & C. A. L. Bailer-Jones 2015), changing their Galactic

<sup>8</sup> As we see later, encounters can be recovered back to a few Myr, compared with the ISOs’ lifetimes of a few Gyr. As the sample of ISOs grows, the probability of finding one only recently released from its parent star rises.

orbit. Tracing ISO orbits back through the Galaxy remains challenging, however, as small uncertainties in orbital elements and stellar astrometry grow rapidly over time (Q. Zhang 2018), even with *Gaia* (Gaia Collaboration et al. 2016) precision.

In this work, we reconstruct the history of stellar encounters affecting 3I/ATLAS over the past 10 Myr using *Gaia* DR3 astrometry and stellar encounters with known stars currently within 500 pc. Section 2 describes the methodology. Section 3 presents the closest encounters their dynamical effects on the orbit of 3I/ATLAS, and in Section 4 we discuss the results. Section 5 summarizes our conclusions.

## 2. METHODS

To trace the past trajectory of 3I/ATLAS, we adopted the position and velocity computed by R. de la Fuente Marcos et al. (2025) at an epoch prior to its entry into the Solar System ( $\approx 3 \times 10^4$  yr ago), namely:  $\alpha = 295^\circ.043^{+0.003}_{-0.004}$ ,  $\delta = -19^\circ.0704^{+0.0006}_{-0.0005}$ , a heliocentric distance of  $1.7819 \pm 0.0003$  pc, and Cartesian Galactic heliocentric velocities  $(U, V, W) = (-51.233 \pm 0.006, -19.456 \pm 0.004, +18.930^{+0.005}_{-0.006}) \text{ km s}^{-1}$ .

The potential stellar encounters are identified by selecting *Gaia* DR3 sources with high-quality astrometry within 500 pc of the Sun. Only sources satisfying:

- `parallax > 2 mas`
- `parallax_over_error > 10`
- `ruwe < 1.4`
- `visibility_periods_used ≥ 8`

were retained from the *Gaia* Archive query, yielding a total of 13,896,270 stars. Since high-quality radial velocities (RVs) are essential for our kinematic analysis, we supplemented the RVs from the *Gaia* Radial Velocity Spectrometer (RVS; D. Katz et al. 2023) with additional measurements from APOGEE-2 DR17 (Abdurro’uf et al. 2022), LAMOST DR7 (A. L. Luo et al. 2022), GALAH DR3 (S. Buder et al. 2021), RAVE DR6 (M. Steinmetz et al. 2020), and the *Gaia*-ESO DR5 survey (A. Hourihane et al. 2023).

If multiple RV measurements are available for a source, we adopt the one with the lowest associated uncertainty, provided it is within  $10 \text{ km s}^{-1}$  of the median RV for that source. Otherwise, the *Gaia* RVS is provided. Our final sample therefore consists of 3,608,022 sources with 6D initial conditions<sup>9</sup>. We corrected the *Gaia* parallaxes using L. Lindegren et al. (2021) and the proper motions following T. Cantat-Gaudin & T. D.

<sup>9</sup> Since our analysis is restricted to nearby stars ( $< 500$  pc) with small fractional parallax errors ( $\sigma_\varpi/\varpi < 0.1$ ), we can safely estimate distances  $d$  using the inverse of the parallax ( $1/\varpi$ )

Brandt (2021), and increased the parallax uncertainties following J. Maíz Apellániz (2022).

To perform the orbital traceback, we used `Gala`, a Python package for galactic dynamics (A. M. Price-Whelan 2017). For the Galactic potential, we adopted `MilkyWayPotential2022`, which includes a spherical nucleus and bulge, a sum of Miyamoto-Nagai disks, and a spherical NFW halo, fit to the A.-C. Eilers et al. (2019) rotation curve. To transform the heliocentric reference frame into the galactocentric one, we adopted the solar distance  $R_0$  to the galactic center as 8.122 kpc (GRAVITY Collaboration et al. 2018), the Solar velocity relative to the Local Standard of Rest (LSR) as  $(U_\odot, V_\odot, W_\odot) = (11.1, 12.24, 7.25) \text{ km s}^{-1}$  (R. Schönrich et al. 2010), an LSR velocity of  $V_C(R_0) = 229 \text{ km s}^{-1}$  (A.-C. Eilers et al. 2019), and a Solar height above the Galactic plane of  $Z_\odot = 20.8 \text{ pc}$  (M. Bennett & J. Bovy 2019).

We first integrated the orbits of both 3I/ATLAS and the *Gaia* DR3 sources backward in time for 100 Myr, with  $10^4$  time steps of  $\Delta t = 0.01 \text{ Myr}$ . Because we found excessively large errors beyond  $-10 \text{ Myr}$ , we repeat the integration up to  $t = -10 \text{ Myr}$  and with a finer time step ( $\Delta t = 1000 \text{ yr}$ ). We also performed a longer 12 Gyr integration of the orbit of 3I/ATLAS to ensure we had captured its maximum  $Z$ -excursions.

To overcome memory and computational limitations, we split the bulk sample into onion-like layers with outer boundaries at 100, 150, 200, 250, 300, 350, 400, 450, and 500 pc and progressively performed our calculations on each layer. A potential close encounter is defined as the time step  $t$  at which the Euclidean distance between 3I/ATLAS and a given star ( $d_{\text{rel}}$ ) falls below the adopted *critical radius*,  $r = 2 \text{ pc}$ , corresponding to the maximum distance at which a passing star can significantly perturb a comet (e.g., Torres, S. et al. 2019; S. Portegies Zwart et al. 2021). This is also roughly the same size as the Hill radius where the star's gravity dominates over the Galactic potential in a corotating frame. We identified 93 nominal stellar encounters (after discarding 14 sources with  $|RV| > 500 \text{ km s}^{-1}$ ).

To account for uncertainties in the initial conditions, arising primarily from the RVs, we re-integrated the orbits of these candidate stars, drawing  $10^3$  Monte Carlo (MC) realizations of their orbits from Gaussian distributions of their uncertainties, including covariances between the astrometric parameters. For 3I/ATLAS, where some solutions show asymmetric errors, we used the largest one for the sampling. Finally, we defined high-confidence close encounters as those for which at least 95% of the sampled orbits approached within the critical radius.

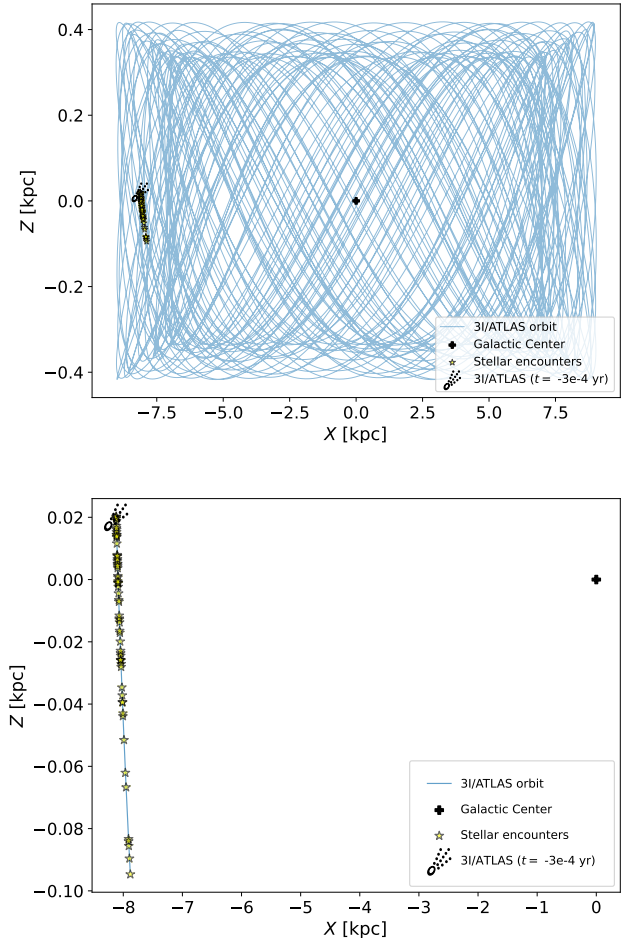


**Figure 1.** Galactic trajectory of 3I/ATLAS integrated 12 Gyr Myr backward in time, projected onto the Galactic XY plane. Stars mark the 62 high-confidence encounters identified in this work. The error bars for both the stars and the cometary orbit are not visible, as they are smaller than the plotted symbols.

### 3. ENCOUNTER HISTORY OF 3I/ATLAS

After propagating the orbit of 3I/ATLAS for 12 Gyr the object reached a maximum Galactic altitude of  $|Z| \approx 420 \text{ pc}$ , placing it near the boundary of the thin disk (K. Vieira et al. 2023; H. Tian et al. 2024). Figure 1 shows the close encounters with respect to the 3I/ATLAS' orbit projected in the XZ Galactic plane. Our Galactic trajectory is in strong agreement with that computed by S. Kakharov & A. Loeb (2025).

We identified 62 high-confidence stellar encounters of 3I/ATLAS in the first 10 Myr (Table 1). To estimate the dynamical influence of these stellar flybys, we adopt the *Classical Impulse Approximation* (CIA; H. Rickman 1976; J. Binney & S. Tremaine 2008). Although based on a simple assumption, the CIA provides a useful first-

order diagnostic for assessing whether 3I/ATLAS experienced an encounter strong enough to significantly alter its trajectory, without the need of performing a full  $N$ -body integration. This approach assumes rectilinear stellar motion and treats the encounter as an instantaneous perturbation, which is valid given that the duration of the encounter is short compared to the comet's dynamical timescale. In this framework, a passing star of mass  $M_\star$  and relative velocity  $v_{\text{rel}}$  imparts an instantaneous change in the velocity of the comet at closest approach. For an encounter with impact parameter  $d_{\text{rel}}$ , the instantaneous velocity kick imparted during the flyby,  $\Delta v$ , can be expressed as,  $|\Delta v| = \frac{2GM_\star}{d_{\text{rel}}v_{\text{rel}}}$ , where  $G$  is the gravitational constant. It is convenient to express the encounter strength in a dimensionless form by normalizing the impulse to the relative velocity, which yields the effective deflection angle of the hyperbolic trajectory,  $\theta \equiv \frac{|\Delta v|}{v_{\text{rel}}}$  (J. Binney & S. Tremaine 2008). Here,  $\theta$  denotes the angular deflection of 3I/ATLAS' velocity vector caused by the flyby. For typical relative velocities of  $V_\infty \sim 20\text{--}60 \text{ km s}^{-1}$ , the value of  $\theta$  quantifies the dynamical strength of the encounter, ranging from very weak ( $10^{-6} \leq \theta < 10^{-5}$ ), through moderate ( $10^{-4} \leq \theta < 10^{-3}$ ), to very strong  $\theta \geq 10^{-2}$  (corresponding to au-scale flybys). These values correspond to impact parameters of  $\sim 0.5 \text{ pc}$  for very weak encounters, and  $\sim 10^3 \text{ au}$  for strong ones. Thus, only encounters within  $\lesssim 10^3\text{--}10^4 \text{ au}$  and/or with very low relative velocities can produce dynamically significant deflections (Torres, S. et al. 2019). At parsec-scale distances, even solar-mass stars yield  $\theta \sim 10^{-6}$ , corresponding to  $\text{sub-m s}^{-1}$  perturbations which are negligible for 3I/ATLAS' Galactic trajectory.

We computed  $|\Delta v|$  and  $\theta$ , deriving stellar masses via cubic-spline interpolation of the de-reddened color  $(G_{BP} - G_{RP})_0$  using the updated M. J. Pecaut & E. E. Mamajek (2013) tables<sup>10</sup>. To deal with the extinction and reddening we used the package `dustmaps` (G. Green 2018) and the R. H. Leike et al. (2020) 3D dust map to obtain the color excess  $E(B - V)$  for each source. Subsequently, we used the `dust-extinction` (K. D. Gordon 2024) library and the K. D. Gordon et al. (2023) extinction law to obtain the final values. As shown in Figure 2, all the stars with close encounters lie on the main sequence (MS), and most of them are already identified as so in the Extended Stellar Parametrizer for Hot Stars (ESP-HS, O. L. Creevey et al. 2023).

In Table 1, we report the deflection angles produced by close stellar encounters within 500 pc over the past 10

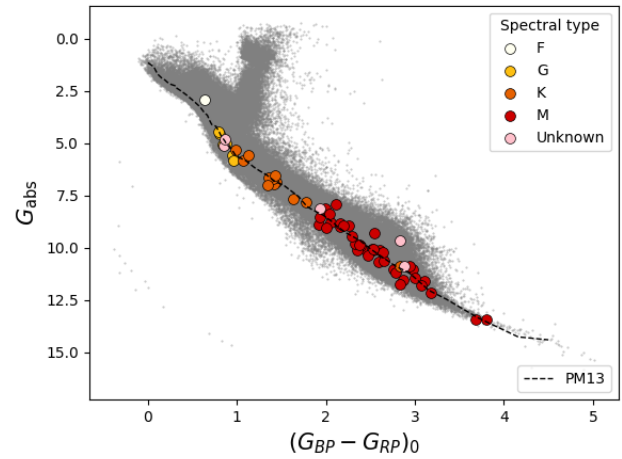


**Figure 2.** Position on the Gaia CMD diagram of the stars that experienced a close encounter with 3I/ATLAS, with spectral types indicated in the legend that comes from O. L. Creevey et al. (2023). The background shows all the sources from our *Gaia* DR3 500 pc sample with available RVs, after applying the same magnitude and parallax error cuts as for the encounter stars. The dashed line marks the MS-locus defined in (M. J. Pecaut & E. E. Mamajek 2013, PM13 in the legend).

Myr on the trajectory of 3I/ATLAS. We find deflection angles on the order of  $10^{-5}\text{--}10^{-6}$  for most of the stars, showing that none of these encounters had a significant impact on 3I/ATLAS's trajectory.

The strongest encounter in our sample was with the star *Gaia* DR3 6863591389529611264, which passed within 0.30 pc of 3I/ATLAS at a relative velocity of  $35 \text{ km s}^{-1}$ , about 72,000 yr ago. This flyby induced a velocity change of only  $\Delta v \simeq 5 \times 10^{-4} \text{ km s}^{-1}$ , corresponding to a deflection angle of  $\theta \simeq 1.6 \times 10^{-5}$ . Equivalently, this would result in a position deviation of only  $\sim 0.05 \text{ pc}$  after 100 Myr. Such a small perturbation indicates that 3I/ATLAS has not been significantly influenced by encounters with stars with known kinematics over the past 4.27 Myr (the epoch of the earliest encounter identified in this work).

For clarity, we present in Figure 3 the probability density-distribution of  $v_{\text{rel}}$  and  $d_{\text{rel}}$  between 3I/ATLAS and the four strongest encounters (those with the greater  $\theta$ , in descending order). They are *Gaia* DR3 6863591389529611264 (A,  $M_A \approx 0.70M_\odot$ ), *Gaia* DR3 6731311275891314304 (B,  $M_B \approx 0.98M_\odot$ ), *Gaia* DR3 1197546390909694720 (C,  $M_C \approx 0.52M_\odot$ ), and *Gaia* DR3 4591398521365845376 (D,  $M_D \approx 0.20M_\odot$ ). As Figure 3 illustrates, although they involve very small relative distances, their relative velocities are always greater than  $15 - 20 \text{ km s}^{-1}$ .

<sup>10</sup> [https://www.pas.rochester.edu/~emamajek/EEM\\_dwarf\\_UBVIJHK\\_colors\\_Teff.txt](https://www.pas.rochester.edu/~emamajek/EEM_dwarf_UBVIJHK_colors_Teff.txt)

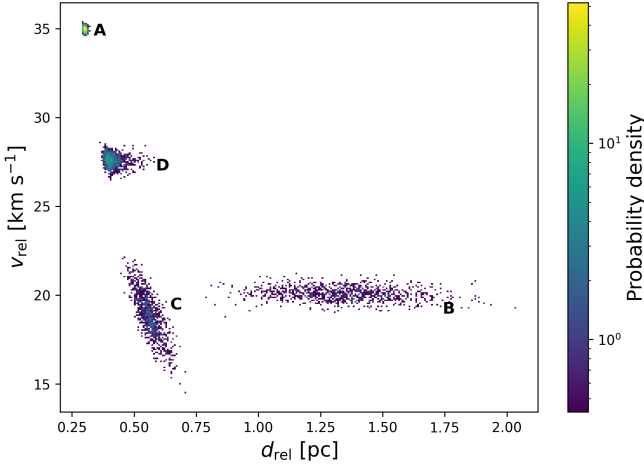


**Figure 3.** Relative velocity  $v_{\text{rel}}$  as a function of relative distance  $d_{\text{rel}}$  for the four strongest encounters obtained from  $10^3$  Monte Carlo orbits.

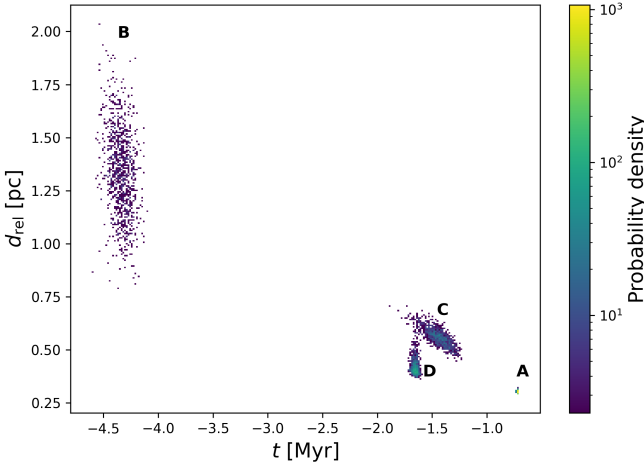


**Figure 4.** Relative distance  $d_{\text{rel}}$  as a function of time  $t$  for the four strongest encounters obtained from  $10^3$  Monte Carlo orbits.

In addition to this, Figure 4 shows the probability density distribution of  $d_{\text{rel}}$  as a function of encounter time  $t$ . The dispersion in relative distance increases with the integration time, especially for  $t < -1$  Myr (as seen for encounter B).

### 3.1. Completeness of the Encounter Sample

To assess the number of stellar encounters that may have been missed—primarily due to the lack of precise RV measurements—we followed the procedure described in [J. L. Gragera-Más et al. \(submitted\)](#).

As a first approximation, the total number of stellar encounters  $N$  expected over a time span  $t$ , within a cylindrical volume of cross section  $\pi r^2$ , can be estimated from the stellar density in the solar neighborhood  $\rho_{\text{ST}}$

(which, as is well known, depends strongly on the spectral type), and their characteristic encounter velocity  $v_{\text{ST}}$ . The latter is given by  $v_{\text{ST}} = \sqrt{v_{\text{3I/ATLAS,ST}}^2 + \sigma_{\text{ST}}^2}$ , where  $v_{\text{3I/ATLAS,ST}}$  is the mean relative velocity of the stars of a given spectral type and 3I/ATLAS, and  $\sigma_{\text{ST}}$  is the velocity dispersion of that spectral type.

Therefore, we estimate  $N$  within  $r = 2$  pc and a time span of  $t = 4.27$  Myr (the time interval between the first and last close encounter identified in our work), as

$$N = \sum \pi r^2 t v_{\text{ST}} \rho_{\text{ST}}. \quad (1)$$

Using  $v_{\text{3I/ATLAS,ST}}$  from [H. Rickman et al. \(2008\)](#) (originally computed for the Sun, but transformed here to the 3I/ATLAS reference frame), together with  $\rho_{\text{ST}}$  and  $\sigma_{\text{ST}}$  from [Torres, S. et al. \(2019\)](#), we obtain  $N = 246$  expected encounters, of which we are reporting approximately  $\sim 25\%$ . This fraction is pretty close to the number of RVs available in our sample ( $\sim 31\%$ ) within the heliocentric distance of the most distant encounter ( $\sim 245$  pc).

Although we recognize that the lack of RVs is a limitation for the number of integrated orbits, it is also true that it is highly unlikely that any of the remaining 75% of encounters would affect the orbit of 3I/ATLAS in this time window. Indeed, if we assume  $r = d_{\text{rel}}$  we can combine the CIA, the effective deflection angle of the hyperbolic trajectory equations, and Equation (1) to obtain the expected number of encounters for a given deflection angle  $\theta$ . It is therefore easy to see that the expected number of strong encounters ( $\theta > 10^{-2}$  rad) is nearly zero ( $N = 10^{-5}$ ) for the  $t = 4.27$  Myr time span.

## 4. DISCUSSION

Understanding the origin of 3I/ATLAS is relevant as it could provide rare empirical constraints on how interstellar objects are produced and evolve, testing competing formation scenarios—from tidal disruptions around white dwarfs to exo-Oort cloud ejections—and, through its kinematics, it directly informs our picture of how planetary material is distributed and recycled across the Galaxy.

Throughout our kinematic study of 3I/ATLAS within the Galactic potential, we investigated whether it could have been ejected by a nearby star or significantly perturbed by a stellar encounter capable of imparting its present peculiar velocity. By integrating the orbit of 3I/ATLAS 10 Myr backward with *Gaia* DR3 stars, we identified 93 nominal encounters (62 at the  $2\sigma$  level), yet none were capable of producing significant perturbations (Fig. 1). Even the closest *Gaia* DR3 6769021226194779136 (0.27 pc,  $0.19 M_{\odot}$ ) and strongest

*Gaia* DR3 6863591389529611264 (0.30 pc, 0.7  $M_{\odot}$ ) encounter occurred at high relative velocities, leaving 3I/ATLAS's origin unassociated with any specific stellar system. We conclude that 3I/ATLAS has not experienced any stellar flybys within the past 4 Myr, among the stars contained in *Gaia* DR3, that could account for its present trajectory nor its origin. There is a caveat to this analysis provided possible incompleteness, that we estimated from *Gaia*'s coverage of the local 245 pc volume and found it to be only  $\sim 25\%$  complete. However, for the remaining 75%, we present a first approximation analysis based on statistics within 100 pc of the Sun. This analysis shows that a strong encounter ( $\theta > 10^{-2}$ ) was unlikely to occur in any case. This is expected on our understanding of kinematic heating of the Galactic disk, which is caused not by star-star encounters but by their interaction with larger agglomerations of matter such as GMCs, satellite galaxies and spiral arms (e.g., C. G. Lacey 1984; G. Toth & J. P. Ostriker 1992; M. Aumer & J. J. Binney 2009).

We further examine the orbit of 3I/ATLAS by analyzing the extent of its vertical motion in the Galactic disk, and conclude that it most likely originates from the thin disk. Its vertical excursion reaches only  $|Z| \sim 0.42$  kpc (Fig. 1), consistent with the thin-disk scale height and far smaller than the kiloparsec-scale typical of thick-disk stars (e.g., G. Gilmore & N. Reid 1983; T. Bensby et al. 2003; A. Recio-Blanco et al. 2014).

As noted by R. de la Fuente Marcos et al. (2025), the space motions  $(U, V, W) = (-51.2, -19.5, +18.9)$  km s $^{-1}$  correspond to a Toomre velocity of  $T \approx 58$  km s $^{-1}$ , well below the canonical thin/thick-disk division at  $T \sim 70-100$  km s $^{-1}$  (e.g., T. Bensby et al. 2003; B. E. Reddy et al. 2006; A. Recio-Blanco et al. 2014). In addition, applying the T. Bensby et al. 2014 criteria yields an odds ratio of TD/D = 0.04 for membership of the thick versus thin disk, implying that 3I/ATLAS is about 20 times more likely to belong to the thin disc than to the thick disc based purely on kinematics (Appendix B). While this strongly favors thin-disk kinematics, T. Bensby et al. (2014) note that purely kinematic criteria can misclassify a minority of stars, some objects with TD/D < 0.1 exhibit chemical abundance patterns characteristic of the thick disk (e.g.  $\alpha$ -enhancement, low [Fe/H]). In the absence of chemical information for 3I/ATLAS, its classification remains probabilistic. Nevertheless, when combined with its vertical component ( $|Z| \sim 0.42$  kpc) and its location in the Toomre diagram ( $T \approx 55$  km s $^{-1}$ ), the Bensby analysis consistently supports a thin-disk origin for 3I/ATLAS.

A. G. Taylor & D. Z. Seligman (2025) used the age–velocity dispersion relation to infer a median kinematic

age of  $\sim 7$  Gyr for 3I/ATLAS, with a 68% confidence interval of 3–11 Gyr, which is consistent with both a thick disk and thin disk origin. Our classification relies on the present-day phase-space location of 3I/ATLAS relative to Galactic populations, whereas A. G. Taylor & D. Z. Seligman (2025) infers a statistical age. Taken together, these results indicate that while 3I/ATLAS follows a thin-disk orbit in the solar neighborhood, it may nonetheless be an old object, consistent with ejection from a long-lived primordial planetesimal disk in an early-formed system.

The recent study Y. Guo et al. (2025) examined the past stellar encounters of 3I/ATLAS. Although they apply a similar methodology, their list of 25 encounters overlaps with ours in only 13 cases. To address this discrepancy, we re-integrated the orbits of the 20 single sources in common with our initial sample. We find that, while the relative velocities and time of encounters agree with their results, the relative distances exceed 2 pc for 10 of these stars (and the remaining 2 shows a RUWE > 2). To understand and quantify the source of the differing results, in Appendix C we examine three key methodological differences between this study and that of Y. Guo et al. (2025): i) the initial conditions; ii) the *Gaia* systematics and iii) the adopted galactic potential. We find good agreement with Y. Guo et al. (2025) for encounters within the past 1 Myr, whereas at longer look-back times our results diverge, with encounter distances drifting as the integration time increases. This indicates that the robust encounters primarily reflect the astrometric precision of *Gaia* on short timescales, while the discrepancies at earlier epochs arise from the sensitivity of the results to the adopted Galactic potential and mass model.

## 5. SUMMARY AND CONCLUSIONS

The emerging picture from recent studies is that interstellar objects are a heterogeneous population that provide rare observational constraints on planetary system evolution across the Galaxy. For 3I/ATLAS, we find that the 62 close stellar encounters identified in *Gaia* DR3 within 500 pc over the past 10 Myr are too fast and at too large distances to have shaped its current orbit. None of them produced deflections larger than  $10^{-5}$  radians, leaving 3I/ATLAS's trajectory essentially unaffected. We estimated the possible incompleteness of our analysis from *Gaia*'s coverage of the local 245 pc volume and found it to be only  $\sim 25\%$  complete. We also found supporting dynamical arguments that favor a thin-disk origin of 3I/ATLAS. Together, all data indicate that while 3I/ATLAS follows a thin-disk orbit in the solar neighborhood, it may nonetheless be an old object, con-

sistent with ejection from a primordial planetesimal disk in an early-formed system, or from an exo-Oort cloud, and is most likely associated with the transition region between the thin and thick disk, although its origin remains undisclosed.

Our study shows that the encounter history of individual ISOs remains, despite the exquisite astrometric precision of *Gaia*, incomplete and subject to systematic errors in the astrometry and Galactic potential even within a few Myr. Nevertheless, chemodynamic trends may still be revealed once a large sample of ISOs has been observed.

## ACKNOWLEDGMENTS

XPC and ST thank J.L. Gragera-Más and Ylva Götberg, for their valuable feedback and comments. XPC acknowledges financial support from the Spanish National Programme for the Promotion of Talent and its Employability grant PRE2022-104959 co-funded by the European Social Fund. ST acknowledges the funding from the European Union’s Horizon 2020 research and innovation program under the Marie

Skłodowska-Curie grant agreement No 101034413. EV acknowledges support from the *DISCOBOLO* project funded by the Spanish Ministerio de Ciencia, Innovación y Universidades under grant PID2021-127289NB-I00. AJM acknowledges support from the Swedish National Space Agency (Career grant 2023-00146). XPC and MM acknowledge support from the Spanish Ministerio de Ciencia, Innovación y Universidades under grants PID2021122842OB-C22 and PID2024-157964OB-C22; from the Xunta de Galicia and the European Union (FEDER Galicia 2021-2027 Program) Ref. ED431B 2024/21, ED431B 2024/02, and CITIC ED431G 2023/01. This work has made use of data from the European Space Agency (ESA) *Gaia* mission and processed by the *Gaia* Data Processing and Analysis Consortium (DPAC). Funding for the DPAC has been provided by national institutions, in particular, the institutions participating in the *Gaia* Multilateral Agreement.

*Software:* astropy (Astropy Collaboration et al. 2013, 2018, 2022), Matplotlib (J. D. Hunter 2007), NumPy (C. R. Harris et al. 2020), Pandas (T. pandas development team 2020)

## APPENDIX

### A. 3I/ATLAS CLOSE ENCOUNTERS

Table 1 lists the high-confidence stellar encounters identified in this study.

### B. KINEMATIC CLASSIFICATION OF 3I/ATLAS

The Galactic population membership of 3I/ATLAS can be assessed through three complementary kinematic diagnostics, the Toomre diagram, integrals-of-motion diagram ( $E, L_z$ ), and the kinematic classification scheme of T. Bensby et al. (2014). First, the Toomre diagram compares the vertical velocity  $T = \sqrt{U^2 + W^2}$  with the azimuthal velocity  $V_{\text{LSR}}$  relative to the Local Standard of Rest. In Fig. 5 left panel, the shaded regions mark the approximate kinematic domains of the thin disk ( $T \lesssim 70 \text{ km s}^{-1}$ ), thick disk ( $70 \lesssim T \lesssim 180 \text{ km s}^{-1}$ ), and halo ( $T \gtrsim 180 \text{ km s}^{-1}$ ), with reference curves of constant peculiar velocity  $V_{\text{pec}} = \sqrt{U^2 + V^2 + W^2}$ . 3I/ATLAS lies well inside the thin-disk regime, with  $T \approx 55 \text{ km s}^{-1}$  and  $V_{\text{pec}} \approx 58 \text{ km s}^{-1}$ , below the canonical thin/thick-disk boundary at  $T \sim 70\text{--}100 \text{ km s}^{-1}$  and with a vertical displacement of  $|Z| \sim 0.42 \text{ kpc}$  (Fig. 1).

Second, we computed the specific orbital energy ( $E$ ) and vertical angular momentum ( $L_z$ ) following the methodology in Section 2. These were evaluated as  $E = \frac{1}{2}(v_x^2 + v_y^2 + v_z^2) + \Phi(R, z)$  and  $L_z = x v_y - y v_x$ , and normalized by the circular values at the solar radius,  $E_{\text{circ}}(R_0)$  and  $L_{z,\odot} = R_0 V_c(R_0)$ . In Figure 5 right panel, thin-disk stars cluster near  $(L_z/L_{z,\odot}, E/E_{\text{circ}}) \approx (1, 1)$ , while thick-disk and halo stars extend to lower  $L_z$  and higher  $E$ . 3I/ATLAS lies within the thin-disk locus, kinematically indistinguishable from the local disk population.

Finally, we assessed the Galactic population membership of 3I/ATLAS using the kinematic classification scheme of T. Bensby et al. (2014), which refines the earlier criteria of T. Bensby et al. (2003). For each stellar population  $X$  (thin disk, thick disk, halo), the relative likelihood is

$$f_X \propto X_X \exp \left[ -\frac{1}{2} \left( \frac{U^2}{\sigma_{U,X}^2} + \frac{(V - V_{\text{asym},X})^2}{\sigma_{V,X}^2} + \frac{W^2}{\sigma_{W,X}^2} \right) \right], \quad (\text{B1})$$

**Table 1.** Identified stellar encounters within 2 pc of 3I/ATLAS at the  $2\sigma$  level. For each star, we list its *Gaia* DR3 source ID, spectral type (ST), interpolated mass  $M_*$ , time of closest approach  $t_{\text{closest}}$ , median relative distance  $d_{\text{rel}}$  and velocity  $v_{\text{rel}}$  with  $1\sigma$  uncertainties. The final columns gives the median encounter strength  $|\Delta v|$ , and deflection angle  $\theta$ .

<i>Gaia</i> DR3 ID	ST	$M_*$ [ $M_\odot$ ]	$t_{\text{closest}} \pm \sigma_{t_{\text{closest}}}$ [Myr]	$d_{\text{rel}} \pm \sigma_{d_{\text{rel}}}$ [pc]	$v_{\text{rel}} \pm \sigma_{v_{\text{rel}}}$ [km s $^{-1}$ ]	$ \Delta v $ [km s $^{-1}$ ]	$\theta$ [rad]
6769021226194779136	M	0.19	$-0.947 \pm 0.004$	$0.276 \pm 0.016$	$72.11 \pm 0.17$	8.37e-05	1.16e-06
6863591389529611264	K	0.70	$-0.720 \pm 0.003$	$0.303 \pm 0.005$	$34.97 \pm 0.13$	5.71e-04	1.63e-05
6779821003058453120	M	0.18	$-0.331 \pm 0.006$	$0.397 \pm 0.008$	$28.33 \pm 0.47$	1.38e-04	4.87e-06
5944464849163504128	K	0.83	$-1.630 \pm 0.010$	$0.407 \pm 0.136$	$67.54 \pm 0.32$	2.60e-04	3.84e-06
1197546390909694720	M	0.52	$-1.654 \pm 0.020$	$0.408 \pm 0.033$	$27.59 \pm 0.33$	4.00e-04	1.45e-05
4484666797357868288	G	1.05	$-3.910 \pm 0.046$	$0.504 \pm 0.407$	$47.10 \pm 0.51$	3.79e-04	8.05e-06
6855915149098312064	M	0.25	$-0.583 \pm 0.056$	$0.550 \pm 0.052$	$105.18 \pm 9.58$	3.67e-05	3.49e-07
1197546562708387584	M	0.40	$-1.688 \pm 0.057$	$0.555 \pm 0.076$	$27.03 \pm 0.90$	2.29e-04	8.49e-06
4591398521365845376	M	0.20	$-1.440 \pm 0.095$	$0.561 \pm 0.041$	$18.91 \pm 1.22$	1.63e-04	8.64e-06
6482924967749137152	F	1.25	$-2.686 \pm 0.019$	$0.582 \pm 0.353$	$49.04 \pm 0.21$	3.77e-04	7.68e-06
6773261320990713216	M	0.32	$-1.293 \pm 0.127$	$0.583 \pm 0.073$	$68.00 \pm 6.34$	6.96e-05	1.02e-06
6620396322451894656	-	0.55	$-3.983 \pm 0.274$	$0.591 \pm 0.404$	$31.82 \pm 2.10$	2.50e-04	7.86e-06
2386898972054841088	M	0.54	$-0.534 \pm 0.003$	$0.598 \pm 0.004$	$38.60 \pm 0.19$	2.00e-04	5.18e-06
692654877680490880	M	0.43	$-2.154 \pm 0.965$	$0.670 \pm 6.487$	$60.34 \pm 17.12$	9.10e-05	1.51e-06
6640455159755767424	M	0.38	$-2.368 \pm 0.625$	$0.712 \pm 0.526$	$43.64 \pm 9.32$	1.05e-04	2.41e-06
6745564794882995712	M	0.36	$-1.178 \pm 0.063$	$0.712 \pm 0.057$	$90.76 \pm 4.75$	4.79e-05	5.27e-07
2386898937694609920	-	0.24	$-0.506 \pm 0.074$	$0.751 \pm 0.112$	$40.70 \pm 5.51$	6.89e-05	1.69e-06
6780592417841129472	K	0.70	$-2.243 \pm 0.045$	$0.789 \pm 0.127$	$40.12 \pm 0.78$	1.92e-04	4.78e-06
4189858726030433792	M	0.46	$-0.608 \pm 0.006$	$0.805 \pm 0.009$	$67.20 \pm 0.61$	7.23e-05	1.08e-06
4093353529682577152	K	0.70	$-3.943 \pm 0.203$	$0.896 \pm 0.288$	$60.83 \pm 3.12$	1.10e-04	1.81e-06
673131271597112576	M	0.34	$-2.387 \pm 1.015$	$0.938 \pm 2.001$	$36.56 \pm 9.79$	8.48e-05	2.32e-06
6570039342736534784	G	1.02	$-0.837 \pm 0.003$	$0.942 \pm 0.053$	$49.34 \pm 0.12$	1.89e-04	3.83e-06
5079819487844050432	G	0.90	$-1.811 \pm 0.020$	$0.952 \pm 0.243$	$78.03 \pm 0.70$	1.04e-04	1.33e-06
6866660813675237248	K	0.81	$-3.255 \pm 0.110$	$0.979 \pm 0.069$	$72.60 \pm 2.39$	9.79e-05	1.35e-06
5254061535106490112	M	0.13	$-0.030 \pm 0.000$	$0.988 \pm 0.005$	$157.05 \pm 1.23$	6.97e-06	4.44e-08
6512303781003214464	K	0.70	$-1.035 \pm 0.004$	$0.992 \pm 0.086$	$71.97 \pm 0.19$	8.41e-05	1.17e-06
6575069780231675264	M	0.28	$-0.225 \pm 0.002$	$0.994 \pm 0.008$	$32.96 \pm 0.24$	7.30e-05	2.21e-06
5909461003111201792	M	0.41	$-0.779 \pm 0.027$	$1.037 \pm 0.071$	$111.33 \pm 3.77$	3.05e-05	2.74e-07
6849531247148752512	K	0.67	$-2.066 \pm 0.053$	$1.059 \pm 0.050$	$76.17 \pm 1.91$	7.14e-05	9.37e-07
6586084515921321728	M	0.45	$-3.076 \pm 0.173$	$1.111 \pm 0.152$	$38.33 \pm 2.12$	9.01e-05	2.35e-06
6734485286788609664	M	0.36	$-0.082 \pm 0.000$	$1.119 \pm 0.002$	$164.60 \pm 0.27$	1.70e-05	1.03e-07
2661803855688028800	M	0.54	$-0.253 \pm 0.001$	$1.151 \pm 0.006$	$63.64 \pm 0.20$	6.28e-05	9.87e-07
6794047652729201024	M	0.48	$-0.196 \pm 0.001$	$1.168 \pm 0.009$	$48.07 \pm 0.36$	7.42e-05	1.54e-06
4307416074032507136	M	0.55	$-1.705 \pm 0.053$	$1.189 \pm 0.045$	$50.19 \pm 1.57$	7.91e-05	1.58e-06
6813799318266090496	M	0.22	$-2.214 \pm 0.415$	$1.218 \pm 0.203$	$33.48 \pm 5.58$	4.70e-05	1.40e-06
6374877128317186048	K	0.88	$-1.350 \pm 0.005$	$1.224 \pm 0.078$	$87.68 \pm 0.21$	7.02e-05	8.00e-07
4072260704719970944	K	0.59	$-0.220 \pm 0.001$	$1.231 \pm 0.004$	$78.33 \pm 0.22$	5.30e-05	6.77e-07
4075141768785646848	M	0.26	$-0.053 \pm 0.001$	$1.253 \pm 0.012$	$49.94 \pm 0.48$	3.50e-05	7.02e-07
5624302662446291072	K	0.73	$-1.544 \pm 0.020$	$1.253 \pm 0.274$	$124.53 \pm 1.53$	4.02e-05	3.23e-07
669785840773435776	-	0.26	$-0.854 \pm 0.025$	$1.255 \pm 0.070$	$51.01 \pm 1.48$	3.43e-05	6.73e-07
6861605946404195456	M	0.45	$-4.128 \pm 0.380$	$1.267 \pm 0.220$	$33.70 \pm 2.95$	9.16e-05	2.72e-06
4083781765499334400	M	0.52	$-1.206 \pm 0.042$	$1.276 \pm 0.065$	$117.40 \pm 4.08$	3.00e-05	2.56e-07
6640420937456214400	M	0.23	$-0.512 \pm 0.014$	$1.289 \pm 0.040$	$135.15 \pm 3.79$	1.13e-05	8.36e-08
6731311275891314304	G	0.98	$-4.339 \pm 0.081$	$1.334 \pm 0.197$	$20.08 \pm 0.37$	3.15e-04	1.57e-05
6851353515873281536	M	0.36	$-1.818 \pm 0.110$	$1.334 \pm 0.105$	$39.94 \pm 2.36$	5.78e-05	1.45e-06
6690652126172090752	K	0.72	$-1.220 \pm 0.008$	$1.410 \pm 0.074$	$68.06 \pm 0.38$	6.47e-05	9.51e-07
6748488052701979136	M	0.44	$-1.689 \pm 0.089$	$1.451 \pm 0.068$	$54.13 \pm 2.82$	4.77e-05	8.82e-07
6602563858757140992	K	0.25	$-0.783 \pm 0.036$	$1.557 \pm 0.174$	$39.25 \pm 1.81$	3.57e-05	9.10e-07
5143621433184275200	M	0.55	$-0.593 \pm 0.003$	$1.582 \pm 0.018$	$38.78 \pm 0.20$	7.66e-05	1.98e-06
5976042887501445376	M	0.40	$-0.308 \pm 0.002$	$1.597 \pm 0.014$	$105.83 \pm 0.80$	2.06e-05	1.94e-07
2331575021572597504	M	0.35	$-0.636 \pm 0.006$	$1.601 \pm 0.026$	$50.98 \pm 0.45$	3.73e-05	7.33e-07
5853498713190525696	M	0.12	$-0.030 \pm 0.000$	$1.605 \pm 0.005$	$30.76 \pm 0.01$	2.02e-05	6.56e-07
6713373362161524736	M	0.27	$-0.438 \pm 0.018$	$1.619 \pm 0.069$	$129.32 \pm 5.37$	1.10e-05	8.54e-08
5032483416324388480	M	0.34	$-1.738 \pm 0.078$	$1.630 \pm 0.086$	$18.72 \pm 0.82$	9.46e-05	5.05e-06
4283408237650849408	G	0.95	$-0.461 \pm 0.002$	$1.672 \pm 0.045$	$78.94 \pm 0.13$	6.19e-05	7.84e-07
5944732953871170176	G	0.90	$-1.094 \pm 0.006$	$1.672 \pm 0.025$	$99.27 \pm 0.40$	4.64e-05	4.67e-07
6650117736660187136	M	0.22	$-0.150 \pm 0.001$	$1.688 \pm 0.010$	$65.80 \pm 0.39$	1.67e-05	2.55e-07
6771477054134260352	M	0.32	$-0.740 \pm 0.020$	$1.716 \pm 0.047$	$49.72 \pm 1.34$	3.17e-05	6.38e-07
6818312813497758720	M	0.38	$-0.758 \pm 0.012$	$1.759 \pm 0.029$	$62.68 \pm 0.99$	2.97e-05	4.73e-07
4079684229322231040	-	0.98	$-0.134 \pm 0.000$	$1.777 \pm 0.004$	$93.83 \pm 0.13$	5.05e-05	5.38e-07
6718894388002453120	-	0.97	$-0.143 \pm 0.000$	$1.951 \pm 0.012$	$115.01 \pm 0.12$	3.73e-05	3.24e-07
6427708902553822592	M	0.42	$-0.181 \pm 0.001$	$1.965 \pm 0.010$	$68.44 \pm 0.16$	2.67e-05	3.91e-07

where  $(U, V, W)$  are the Galactic velocity components relative to the LSR,  $(\sigma_{U,X}, \sigma_{V,X}, \sigma_{W,X})$  are the velocity dispersions of population  $X$ ,  $V_{\text{asym},X}$  is its asymmetric drift, and  $X_X$  is the local fractional density of that population. The classification is based on the ratio  $\frac{\text{TD}}{\text{D}} = \frac{f_{\text{TD}}}{f_{\text{D}}}$ , which measures how much more likely an object is to belong to the thick disk relative to the thin disk. Using the parameters by T. Bensby et al. (2014) and the measured Galactic velocities of 3I/ATLAS,  $(U, V, W) = (-51.2, -19.5, +18.9) \text{ km s}^{-1}$ , we find  $\frac{\text{TD}}{\text{D}} \simeq 0.04$ , indicating that 3I/ATLAS is about 20 times more likely to belong to the thin disk than the thick disk.

Taken together, these three diagnostics—velocity space (Toomre diagram), orbital integrals ( $E-L_z$ ), and likelihood ratios (Bensby method)—all converge on the same conclusion, 3I/ATLAS is dynamically consistent with the Galactic thin disk, and shows no kinematic evidence of thick-disk or halo origin.

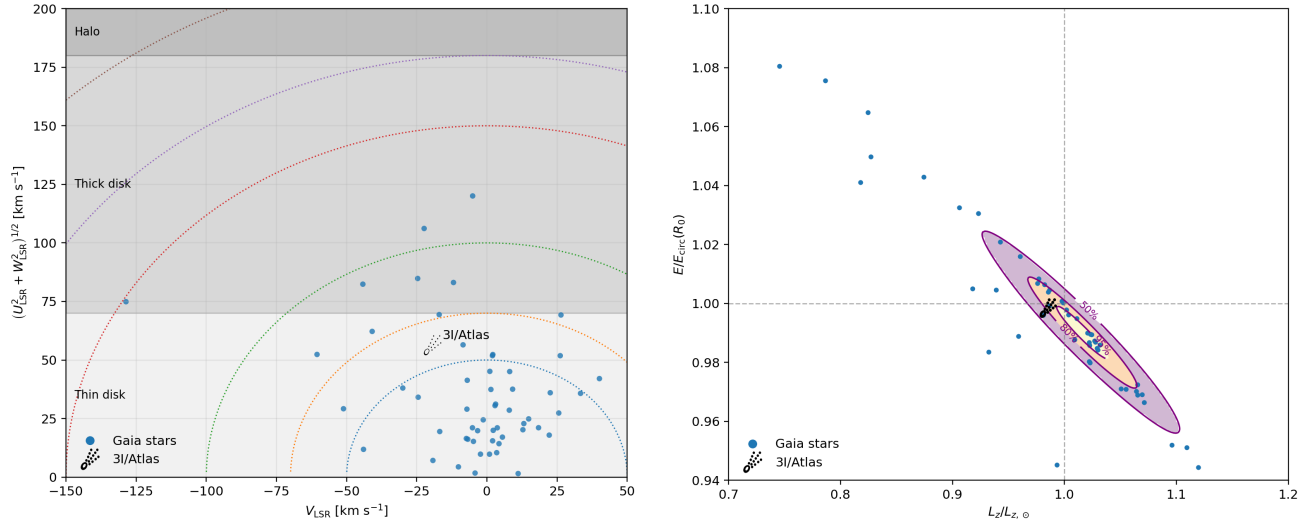


**Figure 5.** Kinematic diagnostics for 3I/ATLAS. *Left:* Toomre diagram for 3I/ATLAS. The vertical axis shows the quadrature of the radial and vertical velocities ( $T$ ) and the horizontal axis the azimuthal velocity. Shaded regions indicate the thin disk ( $T \lesssim 70 \text{ km s}^{-1}$ ), thick disk ( $70 \lesssim T \lesssim 180 \text{ km s}^{-1}$ ), and halo ( $T \gtrsim 180 \text{ km s}^{-1}$ ). *Right:* Specific orbital energy as function of angular momentum for 3I/ATLAS and nearby *Gaia* stars (Table 1). Background density contours (50, 80, and 95%) mark the thin-disk locus in the  $E-L_z$  plane, normalized by the circular orbit at  $R_0$ . The comet symbol represent 3I/ATLAS while, the blue dots the nearby *Gaia* stars.

### C. COMPARISON WITH PREVIOUS STUDIES

The recent study by Y. Guo et al. (2025) identified 25 stellar encounters with 3I/ATLAS within 1 pc. In our analysis, we recover only 13 of these events. To understand the origin of this discrepancy, we highlight three key methodological differences between the two studies: (i) the adopted initial conditions, (ii) the treatment of *Gaia* systematics, and (iii) the choice of Galactic potential.

Y. Guo et al. (2025) adopted as initial conditions the ecliptic heliocentric coordinates for J2016.0 (inbound orbit) computed by JPL Horizons<sup>11</sup>. We instead used the position and velocities of 3I/ATLAS prior to its entry into the Solar System (unbound orbit) as it was calculated by R. de la Fuente Marcos et al. (2025). To evaluate the impact of this choice, we re-integrated their sources using both our initial conditions and theirs. We found no significant differences in the resulting outputs (a few tenths of a pc, as expected as the velocities differ by  $\approx 0.1 \text{ km s}^{-1}$ ).

We adopted a similar approach to Y. Guo et al. (2025) when accounting for systematics in proper motions (T. Cantat-Gaudin & T. D. Brandt 2021) and parallaxes (L. Lindegren et al. 2021) (L21); however, Y. Guo et al. (2025) applied an additional parallax bias correction specifically tailored to the Galactic plane ( $|b| < 20^\circ$ , Y. Ding et al. 2024, D24). We found, however, that most of their encounters have  $|b| > 20^\circ$ , in which case only the L21 correction is applied. Moreover, even in the worst-case scenario, the offset between L21 and D24 is only 0.01 mas. Applying this offset to the L21 corrected parallax of the Y. Guo et al. (2025) encounters gives a median error in the relative distance

<sup>11</sup> <https://ssd.jpl.nasa.gov/horizons/app.html>

**Table 2.** Encounter distances in pc of 3I/ATLAS with *Gaia* DR3 6741607618172465152, using four different potentials in **Gala** and two different initial velocities of 3I/ATLAS.

Initial conditions	MilkyWayPotential2022	MilkyWayPotential	LM10Potential	BovyMWPotential
R. de la Fuente Marcos et al. (2025)	6.34	9.74	5.94	9.91
Y. Guo et al. (2025)	8.92	10.16	6.34	10.29

between encounters of just 0.05 pc. Thus, the D24 parallax correction cannot account for the discrepancies between our results.

Finally, in our nominal integrations we reproduce only 13 of the encounters reported by Y. Guo et al. (2025); the rest diverge in distance as time increases. Such discrepancies are expected in long look-back orbit calculations, small differences in astrometry or in the adopted Galactic potential remain negligible over  $\lesssim 1\text{--}2$  Myr but amplify over tens of Myr, shifting closest approaches by several Myr or parsecs. This explains why recent, nearby encounters (13 in our case) are robust and consistent with Y. Guo et al. (2025) work, whereas longer look-back events are highly sensitive to both measurement errors and model assumptions. A further systematic arises because Y. Guo et al. (2025) integrated with the Y. Zhou et al. (2023) potential (Plummer bulge, razor-thin exponential disks, NFW halo), while our nominal runs used the `MilkyWayPotential2022` from **Gala** (spherical nucleus and bulge, a sum of Miyamoto-Nagai disks, and a spherical NFW halo). Although both are smooth and axisymmetric, their disk scale lengths and halo normalizations differ, leading to accumulated systematic offsets as time goes on and explaining much of the mismatch.

To quantify this, we present in Table 2 the nominal encounter distance of 3I/ATLAS with *Gaia* DR3 6741607618172465152 at around -4.5 Myr, which Y. Guo et al. (2025) find to be 0.85 pc. We test both the initial conditions of Y. Guo et al. (2025) and R. de la Fuente Marcos et al. (2025), and use four potentials implemented in **Gala**: `MilkyWayPotential2022` as in our main simulations, `MilkyWayPotential` (J. Bovy 2015), `LM10Potential` (D. R. Law & S. R. Majewski 2010), and `BovyMWPotential` (J. Bovy 2015). We find nominal values ranging from 5.94 to 9.91 pc for both initial conditions R. de la Fuente Marcos et al. (2025) and Y. Guo et al. (2025). While none of these potentials gives a nominal encounter as close as Y. Guo et al. (2025) find, the range over several pc suggests that differences in the potential used may indeed be responsible for our discrepant encounters beyond  $\approx 1$  Myr. In contrast, the effect of changing the initial conditions is not so pronounced. In short, the robust encounters trace *Gaia*'s astrometric precision, while the fragile ones expose the sensitivity to Galactic mass models.

## REFERENCES

Abdurro'uf, Accetta, K., Aerts, C., et al. 2022, *Astrophys. J. Suppl. Ser.*, 259, 35

Astropy Collaboration, Robitaille, T. P., Tollerud, E. J., et al. 2013, *A&A*, 558, A33, doi: [10.1051/0004-6361/201322068](https://doi.org/10.1051/0004-6361/201322068)

Astropy Collaboration, Price-Whelan, A. M., Sipőcz, B. M., et al. 2018, *AJ*, 156, 123, doi: [10.3847/1538-3881/aabc4f](https://doi.org/10.3847/1538-3881/aabc4f)

Astropy Collaboration, Price-Whelan, A. M., Lim, P. L., et al. 2022, *ApJ*, 935, 167, doi: [10.3847/1538-4357/ac7c74](https://doi.org/10.3847/1538-4357/ac7c74)

Aumer, M., & Binney, J. J. 2009, in IAU Symposium, Vol. 254, The Galaxy Disk in Cosmological Context, ed. J. Andersen, Nordströara, B. m., & J. Bland-Hawthorn, 6

Bennett, M., & Bovy, J. 2019, *MNRAS*, 482, 1417, doi: [10.1093/mnras/sty2813](https://doi.org/10.1093/mnras/sty2813)

Bensby, T., Feltzing, S., & Lundström, I. 2003, *A&A*, 410, 527, doi: [10.1051/0004-6361:20031213](https://doi.org/10.1051/0004-6361:20031213)

Bensby, T., Feltzing, S., & Oey, M. S. 2014, *A&A*, 562, A71, doi: [10.1051/0004-6361/201322631](https://doi.org/10.1051/0004-6361/201322631)

Binney, J., & Tremaine, S. 2008, *Galactic Dynamics*: Second Edition (Princeton University Press)

Bovy, J. 2015, *ApJS*, 216, 29, doi: [10.1088/0067-0049/216/2/29](https://doi.org/10.1088/0067-0049/216/2/29)

Brasser, R., & Morbidelli, A. 2013, *Icarus*, 225, 40, doi: [10.1016/j.icarus.2013.03.012](https://doi.org/10.1016/j.icarus.2013.03.012)

Buder, S., Sharma, S., Kos, J., et al. 2021, *Mon. Not. R. Astron. Soc.*, 506, 150

Cantat-Gaudin, T., & Brandt, T. D. 2021, *A&A*, 649, A124, doi: [10.1051/0004-6361/202140807](https://doi.org/10.1051/0004-6361/202140807)

Creevey, O. L., Sordo, R., Paillet, F., et al. 2023, *A&A*, 674, A26, doi: [10.1051/0004-6361/202243688](https://doi.org/10.1051/0004-6361/202243688)

de la Fuente Marcos, R., Alarcon, M. R., Licandro, J., et al. 2025, *A&A*, 700, L9, doi: [10.1051/0004-6361/202556439](https://doi.org/10.1051/0004-6361/202556439)

de León, J., Licandro, J., Serra-Ricart, M., et al. 2019, *Research Notes of the American Astronomical Society*, 3, 131, doi: [10.3847/2515-5172/ab449c](https://doi.org/10.3847/2515-5172/ab449c)

Ding, Y., Liao, S., Wu, Q., Qi, Z., & Tang, Z. 2024, *A&A*, 691, A81, doi: [10.1051/0004-6361/202450967](https://doi.org/10.1051/0004-6361/202450967)

Do, A., Tucker, M. A., & Tonry, J. 2018, *ApJL*, 855, L10, doi: [10.3847/2041-8213/aaae67](https://doi.org/10.3847/2041-8213/aaae67)

Eilers, A.-C., Hogg, D. W., Rix, H.-W., & Ness, M. K. 2019, *ApJ*, 871, 120, doi: [10.3847/1538-4357/aaf648](https://doi.org/10.3847/1538-4357/aaf648)

Feng, F., & Bailer-Jones, C. A. L. 2015, *MNRAS*, 454, 3267, doi: [10.1093/mnras/stv2222](https://doi.org/10.1093/mnras/stv2222)

Gaia Collaboration, Prusti, T., de Bruijne, J. H. J., et al. 2016, *A&A*, 595, A1, doi: [10.1051/0004-6361/201629272](https://doi.org/10.1051/0004-6361/201629272)

Gilmore, G., & Reid, N. 1983, *MNRAS*, 202, 1025, doi: [10.1093/mnras/202.4.1025](https://doi.org/10.1093/mnras/202.4.1025)

Gordon, K. D. 2024, *Journal of Open Source Software*, 9, 7023, doi: [10.21105/joss.07023](https://doi.org/10.21105/joss.07023)

Gordon, K. D., Clayton, G. C., Decleir, M., et al. 2023, *ApJ*, 950, 86, doi: [10.3847/1538-4357/accb59](https://doi.org/10.3847/1538-4357/accb59)

Gragera-Más, J. L., Torres, S., Mustill, A. J., & Villaver, E. submitted,

GRAVITY Collaboration, Abuter, R., Amorim, A., et al. 2018, *A&A*, 615, L15, doi: [10.1051/0004-6361/201833718](https://doi.org/10.1051/0004-6361/201833718)

Green, G. 2018, *The Journal of Open Source Software*, 3, 695, doi: [10.21105/joss.00695](https://doi.org/10.21105/joss.00695)

Guo, Y., Zhang, L., Feng, F., et al. 2025, Search for Past Stellar Encounters and the Origin of 3I/ATLAS, <https://arxiv.org/abs/2509.03361>

Harris, C. R., Millman, K. J., van der Walt, S. J., et al. 2020, *Nature*, 585, 357, doi: [10.1038/s41586-020-2649-2](https://doi.org/10.1038/s41586-020-2649-2)

Heisler, J., & Tremaine, S. 1986, *Icarus*, 65, 13, doi: [10.1016/0019-1035\(86\)90060-6](https://doi.org/10.1016/0019-1035(86)90060-6)

Higuchi, A., & Kokubo, E. 2015, *AJ*, 150, 26, doi: [10.1088/0004-6256/150/1/26](https://doi.org/10.1088/0004-6256/150/1/26)

Hopkins, M. J., Bannister, M. T., & Lintott, C. 2025a, *AJ*, 169, 78, doi: [10.3847/1538-3881/ad9eb3](https://doi.org/10.3847/1538-3881/ad9eb3)

Hopkins, M. J., Dorsey, R. C., Forbes, J. C., et al. 2025b, *ApJL*, 990, L30, doi: [10.3847/2041-8213/adfbf4](https://doi.org/10.3847/2041-8213/adfbf4)

Hopkins, M. J., Lintott, C., Bannister, M. T., Mackereth, J. T., & Forbes, J. C. 2023, *AJ*, 166, 241, doi: [10.3847/1538-3881/ad03e6](https://doi.org/10.3847/1538-3881/ad03e6)

Hourihane, A., François, P., Worley, C. C., et al. 2023, *Astron. Astrophys.*, 676, A129

Hunter, J. D. 2007, *Computing in Science & Engineering*, 9, 90, doi: [10.1109/MCSE.2007.55](https://doi.org/10.1109/MCSE.2007.55)

Jiménez-Torres, J. J., Pichardo, B., Lake, G., & Throop, H. 2011, *MNRAS*, 418, 1272, doi: [10.1111/j.1365-2966.2011.19579.x](https://doi.org/10.1111/j.1365-2966.2011.19579.x)

Kakharov, S., & Loeb, A. 2025, <https://arxiv.org/abs/2408.02739>

Katz, D., Sartoretti, P., Guerrier, A., et al. 2023, *Astron. Astrophys.*, 674, A5

Lacey, C. G. 1984, in *NATO Advanced Study Institute (ASI) Series C*, Vol. 117, *Formation and Evolution of Galaxies and Large Structures in the Universe*, ed. J. Audouze & J. Tran Thanh Van, 351

Law, D. R., & Majewski, S. R. 2010, *ApJ*, 714, 229, doi: [10.1088/0004-637X/714/1/229](https://doi.org/10.1088/0004-637X/714/1/229)

Leike, R. H., Glatzle, M., & Enßlin, T. A. 2020, *A&A*, 639, A138, doi: [10.1051/0004-6361/202038169](https://doi.org/10.1051/0004-6361/202038169)

Levine, W. G., & Laughlin, G. P. 2021, in *American Astronomical Society Meeting Abstracts*, Vol. 238, *American Astronomical Society Meeting Abstracts #238*, 232.07

Lindgren, L., Bastian, U., Biermann, M., et al. 2021, *A&A*, 649, A4, doi: [10.1051/0004-6361/202039653](https://doi.org/10.1051/0004-6361/202039653)

Lisse, C. M., Bach, Y. P., Bryan, S., et al. 2025, <https://arxiv.org/abs/2508.15469>

Luo, A. L., Zhao, Y. H., Zhao, G., & et al. 2022, *VizieR Online Data Catalog: LAMOST DR7 catalogs (Luo+, 2019)*, *VizieR On-line Data Catalog: V/156*. Originally published in: 2019RAA..in.prep..L

Maíz Apellániz, J. 2022, *A&A*, 657, A130, doi: [10.1051/0004-6361/202142365](https://doi.org/10.1051/0004-6361/202142365)

Meech, K. J., Weryk, R., Micheli, M., et al. 2017, *Nature*, 552, 378, doi: [10.1038/nature25020](https://doi.org/10.1038/nature25020)

pandas development team, T. 2020, *pandas-dev/pandas: Pandas*, latest Zenodo, doi: [10.5281/zenodo.3509134](https://doi.org/10.5281/zenodo.3509134)

Pecaut, M. J., & Mamajek, E. E. 2013, *ApJS*, 208, 9, doi: [10.1088/0067-0049/208/1/9](https://doi.org/10.1088/0067-0049/208/1/9)

Portegies Zwart, S., Torres, S., Cai, M. X., & Brown, A. G. A. 2021, *A&A*, 652, A144, doi: [10.1051/0004-6361/202040096](https://doi.org/10.1051/0004-6361/202040096)

Portegies Zwart, S., Torres, S., Pelupessy, I., Bédorf, J., & Cai, M. X. 2018, *MNRAS*, 479, L17, doi: [10.1093/mnrasl/sly088](https://doi.org/10.1093/mnrasl/sly088)

Price-Whelan, A. M. 2017, *The Journal of Open Source Software*, 2, 388, doi: [10.21105/joss.00388](https://doi.org/10.21105/joss.00388)

Rafikov, R. R. 2018, *ApJ*, 861, 35, doi: [10.3847/1538-4357/aac5ef](https://doi.org/10.3847/1538-4357/aac5ef)

Raymond, S. N., Armitage, P. J., Veras, D., Quintana, E. V., & Barclay, T. 2018, *MNRAS*, 476, 3031, doi: [10.1093/mnras/sty468](https://doi.org/10.1093/mnras/sty468)

Recio-Blanco, A., de Laverny, P., Kordopatis, G., et al. 2014, *A&A*, 567, A5, doi: [10.1051/0004-6361/201322944](https://doi.org/10.1051/0004-6361/201322944)

Reddy, B. E., Lambert, D. L., & Allende Prieto, C. 2006, *MNRAS*, 367, 1329, doi: [10.1111/j.1365-2966.2006.10148.x](https://doi.org/10.1111/j.1365-2966.2006.10148.x)

Rickman, H. 1976, *Bulletin of the Astronomical Institutes of Czechoslovakia*, 27, 92

Rickman, H. 2014, *M&PS*, 49, 8, doi: [10.1111/maps.12080](https://doi.org/10.1111/maps.12080)

Rickman, H., Fouchard, M., Froeschlé, C., & Valsecchi, G. B. 2008, *Celestial Mechanics and Dynamical Astronomy*, 102, 111, doi: [10.1007/s10569-008-9140-y](https://doi.org/10.1007/s10569-008-9140-y)

Schönrich, R., Binney, J., & Dehnen, W. 2010, *MNRAS*, 403, 1829, doi: [10.1111/j.1365-2966.2010.16253.x](https://doi.org/10.1111/j.1365-2966.2010.16253.x)

Seligman, D. Z., Micheli, M., Farnocchia, D., et al. 2025, ApJL, 989, L36, doi: [10.3847/2041-8213/adf49a](https://doi.org/10.3847/2041-8213/adf49a)

Steinmetz, M., Guiglion, G., McMillan, P. J., et al. 2020, Astron. J., 160, 83

Taylor, A. G., & Seligman, D. Z. 2025, arXiv e-prints, arXiv:2507.08111, doi: [10.48550/arXiv.2507.08111](https://doi.org/10.48550/arXiv.2507.08111)

Tian, H., Liu, C., Li, J., & Zhang, B. 2024, MNRAS, 531, 1730, doi: [10.1093/mnras/stae1247](https://doi.org/10.1093/mnras/stae1247)

Torres, S., Cai, M. X., Brown, A. G. A., & Zwart, S. P. 2019, Astronomy & Astrophysics, 629, 13, doi: [10.1051/0004-6361/201935330](https://doi.org/10.1051/0004-6361/201935330)

Torres, S., Naoz, S., Li, G., & Rose, S. C. 2023, MNRAS, 524, 1025, doi: [10.1093/mnras/stad1923](https://doi.org/10.1093/mnras/stad1923)

Toth, G., & Ostriker, J. P. 1992, ApJ, 389, 5, doi: [10.1086/171185](https://doi.org/10.1086/171185)

Veras, D., & Tout, C. A. 2012, Monthly Notices of the Royal Astronomical Society, 422, 1648, doi: [10.1111/j.1365-2966.2012.20741.x](https://doi.org/10.1111/j.1365-2966.2012.20741.x)

Veras, D., Wyatt, M. C., Mustill, A. J., Bonsor, A., & Eldridge, J. J. 2011, Monthly Notices of the Royal Astronomical Society, 417, 2104, doi: [10.1111/j.1365-2966.2011.19393.x](https://doi.org/10.1111/j.1365-2966.2011.19393.x)

Vieira, K., Korchagin, V., Carraro, G., & Lutsenko, A. 2023, Galaxies, 11, doi: [10.3390/galaxies11030077](https://doi.org/10.3390/galaxies11030077)

Xing, Z., Oset, S., Noonan, J., & Bodewits, D. 2025, arXiv e-prints, arXiv:2508.04675, doi: [10.48550/arXiv.2508.04675](https://doi.org/10.48550/arXiv.2508.04675)

Zhang, Q. 2018, ApJL, 852, L13, doi: [10.3847/2041-8213/aaa2f7](https://doi.org/10.3847/2041-8213/aaa2f7)

Zhang, Y., & Lin, D. N. C. 2020, Nature Astronomy, 4, 852, doi: [10.1038/s41550-020-1065-8](https://doi.org/10.1038/s41550-020-1065-8)

Zhou, Y., Li, X., Huang, Y., & Zhang, H. 2023, ApJ, 946, 73, doi: [10.3847/1538-4357/acadd9](https://doi.org/10.3847/1538-4357/acadd9)